Effortless Production, Characterization of Cu/Cu2O Nanostructures using Coconut Water (Cocos nucifera L.) as Bioreductants towards Antibacterial, Antioxidant, and Cytotoxicity on A549 & HeLa Cell lines

Anbalagan Srinivasan
Government Arts College (Autonomous), Coimbatore-641018, Tamil Nadu, India
Gopalakrishnan Gayathri
Anna University Regional Campus
Sivasdasan Devipriya
VIT University
Nanjan Velmani
Government Arts College (Autonomous), Coimbatore-641018, Tamil Nadu, India
Guruswamy Rajagopal
Government Arts College (Autonomous), Coimbatore-641018, Tamil Nadu, India
Kamaludeen Balkis Ameen
Herbiomes Private Limited
Arokiam Joseph Clement
Government Arts College (Autonomous), Coimbatore-641018, Tamil Nadu, India
Perumal Pandaram
Kudankulam Nuclear Power Project, Kudankulam–627 116,
Krishnan Rajasekar
Anna University Regional Campus
Ramasubbu Alagunambi (alagunambiramasubbu@gacbe.ac.in)
Government Arts College (Autonomous), Coimbatore-641018, Tamil Nadu, India

Research Article

Keywords: Heterogeneous nanosturctures, liquid endosperm, biocide, radical scavengers, lung cancer, cervical cells

Posted Date: October 4th, 2023

DOI: https://doi.org/10.21203/rs.3.rs-3380313/v1

Additional Declarations: No competing interests reported.

Abstract

Facile fabrication of Copper/Cuprous Oxide Nanostructures (Cu/Cu_2O-NS) using Fehling's solution and Tender, Matured Coconut water (TCW & MCW); *Cocos nucifera*) as bio-reductants was accomplished. The bio-fabricated nanostructures displayed the distinctive SPR bands confirming the formation of Cu/Cu_2O-NS. The powder X – ray diffraction studies showed the FCC crystal pattern of copper with co-existence of cuprous oxide. The morphology of synthesized Cu/Cu_2O-NS was analyzed with the help of FE-SEM and HR-TEM analysis. The DLS measurements indicated negative zeta potential (ζ) values, which endorsed the colloidal stability of Cu/Cu_2O-NS. The BET surface area analysis demonstrated that both Cu/Cu_2O-NS possessed a mesoporous structure as confirmed by N_2 sorption isotherms, the pore size distribution analysis was carried out by BJH method. The bio-fabricated Cu/Cu_2O-NS exhibited the remarkable antibacterial efficacy against Gram + Ve and Gram –Ve bacteria. The antioxidant capability of Cu/Cu_2O-NS was assessed through DPPH free radical scavenging assay. The anticancer potential of synthesized Cu/Cu_2O-NS was evaluated against Lung and Cervical Cancer Cell lines using MTT assay. The apoptotic assessments were performed by fluorescence microscopy with AO/EB staining. The results showed that MCW-Cu/Cu_2O-NS exhibited higher potency compared to TCW-Cu/Cu_2O-NS. Flow cytometry analysis showed that the maximum concentration of (50 µg/ml) of MCW-Cu/Cu_2O-NS inducted the highest level of apoptosis. Overall the results highlighted the potential of bio-fabricated Cu/Cu_2O-NS against specific bacterial strains as well as Lung and Cervical Cancer cell lines.

1. Introduction

In recent years, researchers are putting efforts in development of efficient green chemistry strategies for the synthesis of nanostructured materials. In particular, green engineered metal and metal oxide nanostructures have gained attention due to their inimitable biomedical and environmental applications [1–8]. Notably, the copper based nanostructures have gained much interest because of their biocompatibility, economic viability and flexible applications [4, 9–11]. The competence of copper nanostructures is owing to their huge aspect quotient compared to the bulk counter parts. This property enhances the shelf life and entry into the living system with ease [3, 12, 13]. Various approaches have been reported for the production of Cu/Cu_2O-NS such as sonochemcial [14], solvothermal [15], electrochemical [16], and wet chemical synthesis [17, 18]. The above methods are very expensive, requiring complex steps and causing toxic intermediates that may have harmful effect on humans and environment. Hence, many eco-benign approaches were considered to reduce the harmful effects [19]. Many plants such as *Citrus sinensis* [20], *Prosopis cineraria* [21], *Cassia fistula* [22], *Celastrus paniculatus* [23], *Prunus nepalensis* [24], *Allium noeanum* [25], *Prunus mahaleb* L. [26], *Phoenix dactylifera* L. [27], *Musa paradisiacal* L [28], *Vicia faba* [29], *Cynara scolymus* L.[30] were used to synthesize copper based nanostructures.

Coconut (*Cocos nucifera* L.) affiliated to the family Arecaceae, the liquid endosperm (coconut water) is a simple liquid with a sweet and salty in taste. Chemical analysis of coconut endosperm revealed its

nutrient source and electrolytes like calcium, potassium, magnesium, and iron. In addition natural sugars, vitamin C and fatty acids also reported [31]. In folk medicine, coconut water is an herbal drink with medicinal use to treat various ailments of human including headaches, stomach upset, fever, diarrhea and dysentery among ethnic groups [32]. It is also reported to have anti-diabetic, anti-inflammatory, antibacterial, wound healing and anti-thrombotic activity [33, 34]. Further, the wide range of applications of coconut water in bio-medical field is owing to its enzymes like phosphatase, catalase, diastase and phytohormones [35].

There are several bacterial pathogens that are responsible for complicated diseases and infections. In this regard, surface modified copper based nanostructures may offer promising applications [36–38]. The bio molecule functionalized metal/metal oxide nanostructures have been found to enhanced antioxidant activity; especially copper based nanostructures have fascinated momentous attention due their unique potentials [27]. Cancer is another dreadful disease that leads the death if not timely treated. The treatment of cancer by various green engineered nanostructures may provide harmonious anticancer effect on the cancer cells and also enhanced drug delivery to the targeted cancer regions [24, 25, 37, 38].

The careful perusal of reported articles disclosed that no studies have been done and reported on biosynthesis of copper based nanostructures by using coconut water as bioreductant. So, this study happens to be the first of this kind; and also it is an effortless and economically viable method for the production of Cu/Cu_2O-NS. The present work deals the biological activity of green synthesized Cu/Cu_2O-NS. The anti-bacterial activity was evaluated against Arthrobacter sp. (Gram + Ve) and *Escherichia coli*, *Klebsiella pneumonia* (-Ve) bacteria. An anti-oxidant activity was performed using the DPPH free radical scavenging method, and anticancer activity was assessed using Lung cancer and cervical cancer cell lines.

2. Experimental Section

2.1. Materials

All the chemicals viz., $CuSO_4.5H_2O$, $KNaC_4H_4O_6.4H_2O$, NaOH, etc. which were of analytical grade from Merck, Hi-media, S-d Fine Chemicals, and all were used without any further purification. The fresh coconut water i.e liquid endosperms of 100 ml was collected in a well cleaned Erlenmeyer Flasks from the tender / mature coconuts which were harvested in the local agricultural farm located in Coimbatore and used for synthesis of Cu/Cu_2O-NS after filtration.

2.2. Synthesis of Cu/Cu_2O Nanostructures

In this “bottom-up” bio-reduction procedure, the Cu/Cu_2O-NS were constructed from atoms and molecules by eco-friendly approach. In this typical procedure, 100 ml of farm fresh coconut water (Both Tender coconut water (TCW) and Matured coconut water (MCW) each was taken in a 250 ml Iodine flask separately. Fehling's solutions (contains 2×10^{-3} M $CuSO_4.5H_2O$) was added drop wise through a

dropping funnel into an Iodine flask (250 ml) which contains 100 ml of TCW or MCW and it was kept under vigorous stirring over a period of 15 min. This freshly prepared mixture was under constant stirring for a further 15 min at room temperature to achieve homogeneous mixture of stable Cu/Cu_2O-NS. The visible exhibition of fluorescent green color by the mixture in the flask revealed the formation of copper nanoparticles, which on subsequently turned into a stable cuprous oxide system over time (10–15 min). The final products of copper/cuprous oxide nanostructures (Cu/Cu_2O-NS) were separated by centrifugation of the mixture at 8000 rpm for 3 min and washed several times with doubly distilled water. The obtained products were dried in a hot air oven at 70 ˚C for 6 hr to eliminate the moisture from the product. The procedure was repeated for TCW as well as MCW under similar experimental conditions to confirm similarity of results. The synthesized nanostructures were subsequently confirmed by subjecting into various physicochemical investigations.

2.3. Characterizations

The Surface Plasmon Resonance (SPR) profile of the synthesized Cu/Cu_2O-NS was evaluated by UV-Vis. Spectrophotometer (Carry 8454, Agilent Technologies, USA). The morphologies and elemental compositions of synthesized Cu.Cu_2O-NS were analyzed using SEM & EDS, by a LEO 1455 VP. Philips analytical X-Ray diffractometer (Cu Kα radiation λ = 1.54 Å) was used to examine the crystal pattern of the samples. The High Resolution Transmission Electron Microscopy (HR-TEM) images and Selected Area Electron Diffraction (SAED) patterns for synthesized samples were obtained using a JEOL 2100 LaB_6 TEM (200kV). HR-TEM samples were prepared by dipping the suspension onto carbon coated TEM grids (Ted Pella, Redding, USA) and let the carrier to disappear in air. The Brunauer Emmett Teller (BET) isotherms, total surface area and pore size distribution of the samples were carried out using NOVAWIN Quantachrome 1200e surface area analyzer.

2.4. Biological Screening of Cu/Cu_2O-NS

2.4.1. Antibacterial activity

Antibacterial potential of the synthesized samples were determined against Arthobacter sp (Gram + Ve) and *Escherichia coli*, *Klebsiella pneumoniae* (Gram –Ve) bacterial strains by Agar well diffusion method [4]. In brief, wells were formed by punching the nutrient agar surface with sterile steel borer (4–5 mm). The suspension of green synthesized Cu/Cu_2O-NS was added into the wells at different concentrations (5–20µg/ml). The Petri dishes were incubated at 35˚C ± 2˚C for 24 hr, and the zones of inhibition were measured in millimeter. Double distilled water was used as negative control whereas streptomycin was used as a positive control.

2.4.2. Antioxidant activity

The radical scavenging ability of the green synthesized Cu/Cu_2O-NS against DPPH stable free radical was conducted by adopting the reported method with slight modification [27]. In brief, 1×10^{-4} M DPPH solution was made by dissolving 4 mg of DPPH in 100 ml methanol (AR grade) and stored in refrigerator.

The radical scavenging was monitored at 517 nm at different concentrations (20–100 µg/ml) of the suspension of the Cu/Cu_2O-NS. After an 30 min at room temperature (incubation period), the absorbance at 517 nm was measured. The percentage of radical scavenging activity for each sample was calculated by using the following equation (Eq. 1).

$$\%\mathrm{Scavening} = \frac{\mathrm{ODofcontrol} - \mathrm{ODoftestsample}}{\mathrm{ODofcontrol}} \times 100$$

2.4.3. Cytotoxicity studies

2.4.3.1 Cell culture condition

The A549 and HeLa cell lines were procured from NCCS, Pune, INDIA. The obtained cells were conserved in McCoy's medium and complemented with Fetal Calf Serum, 1- glutamine (2×10^{-3} M) and balanced salt solution adjusted to contain Sodium carbonate (1.5 g/L), 1×10^{-3} M of nonessential amino acids, 1×10^{-3} M of sodium pyruvate, 1- glutamine (2×10^{-3} M), glucose (1.5 g/L), HEPES (1×10^{-2} M) and Fetal Bovine Serum (FBS). Penicillin and streptomycin (100 IU/ 100µg) were adjusted to 1ml/L. The cells were preserved at 37 ˚C with 5% CO_2 atmosphere.

2.4.3.2. Evaluation of Cytotoxicity

The half maximal inhibition concentration (IC_{50}) was determined by using the MTT assay [21]. A population of 10,000 cancer cells was cultivated in a 96 well plate over 48 hr. After replacing the media with fresh one containing samples, the cells were cultured for a further 48 hr. The culture medium was then taken out of each well and 100 µl of the MTT solution was added. Each well was then incubated at 37 ˚C for 4 hr. After removing the supernatant from each well, 50 µl of DMSO was added and incubated for 10 min to dissolve the formazan crystals. In an ELISA multiwall plate reader, the optical density was measured at 620 nm. The following formula (Eq. 2) was used to get the percentage of viability using the optical density value.

$$\%\mathrm{Viability} = \frac{\mathrm{ODofExperimentalsample}}{\mathrm{ODofExperimentalcontrol}} \times 100$$

2

2.4.3.3. Apoptotic Assessment (Fluorescence Microscopic analysis)

On clean microscope cover slips, 0.9 ml of the cell suspension (100000 cells/ml) was comibined with around 100 µl of the Acridine orange and Ethidium bromide mixture (each 100 mg/ml). the pre treated cancer cells were gathered with various samples, washed in PBS (pH = 7.2), and stained with 10 µl of AO/EB. The cells were incubated for 2 min, twice rinsed in PBS, and then seen under fluorescence microscope using a 480 nm excitation filter.

2.4.3.4. Cell cycle analysis (Flow cytometry)

Different sample concentrations were applied to selected cell lines (2,00,000 cells/ 10 cm plate) for a period of 24 hr. Centrifugation was used to separate the cells which were then washed in ice cold PBS solutions and resuspended in ice-cold ethanol (70%) before use. RNase (10 µg/ml) was applied to the washed cells at 37 ˚C, followed by centrifugation and 30 min of propidium iodide staining. Then, using flow cytometry, the DNA concentration was determined.

3. Results and Discussion

3.1. UV-Visible spectrophotometric studies

Figure 1 illustrates the UV-Visible spectra of (a) TCW-Cu/Cu_2O-NS; (b) MCW-Cu/Cu_2O-NS; (c) Pure Fehling's solution; [(d) Pure TCW; (e) Pure MCW (inset)]. The absorption spectrum of TCW-Cu/Cu_2O-NS has a peak at 493 nm with shoulder at 467 nm (Fig. 1.a). These molecular like optical absorption bands arise due to the anisotropic shape of the particles and confirm the octahedral pattern. The present study confirms the Mie's theory that spherical nanoparticles are expected to exhibit a single SPR peak, whereas particles with anisotropic shape (TCW-Cu/Cu_2O-NS) may yield two or more SPR peaks, depending on particle shape [6, 39, 40]. Figures (1.b) shows the absorption profile of the MCW-Cu/Cu_2O-NS which is ascribed to the inter band electronic transitions of the copper clusters due to the discrete energy levels. The wide absorbing band peaked at 503 nm because cuprous oxide is a narrow band gap semiconductor which has good agreement with existing reports [7, 14, 41]. The reason behind the small difference between the SPR bands of TCW-Cu/Cu_2O-NS and MCW-Cu/Cu_2O-NS is due to the facet dependent optical properties [6]. Figures (1. c) shows the absorption spectrum of pure Fehling's solution, the broad peak centered at 672 nm ascribed to the electronic transition (d-d) of Cu^{2+} ions [42]. The major absorption peaks (Fig. 1. inset) were observed at 199 nm and 217 nm in both TCW and MCW are corresponding to simple reducing sugars present in coconut water [43]. The role of simple reducing sugars and its reduction mechanism has been given in scheme 1. Subsequently the absorption maximum at 267 nm indicates the n-π* conjugated electrons of furan based heterocycle (ascorbic acid). The characteristic peak of ascorbic acid at 267 nm slightly red shifted to 298 nm (in both TCW-Cu/Cu_2O-NS and MCW-Cu/Cu_2O-NS), this shift may be due to the Cu^{2+} ions oxidize the ascorbic acid (scheme S1) [44]. An estimate of the band gap is obtained using the Tauc plot, the optical band gaps were found to be 2.41 eV and 2.06 eV for TCW-Cu/Cu_2O-NS and MCW-Cu/Cu_2O-NS respectively (Fig. S1). The obtained band gaps are consistent with existing literatures [19, 28].

(Fig. 1) **(Scheme 1)**

3.2. Powder X-Ray Diffraction studies (p-XRD)

The crystal pattern of synthesized samples was confirmed by p-XRD analysis (Fig. 2). The TCW-Cu/Cu_2O-NS shows the high intense diffraction peaks [2θ at 28.80˚ (110), 35.67˚ (111), 41.57˚ (200), 60.68˚ (220) and 76.73˚ (222) revealed the cubic phase of Cu_2O (Fig. 2. a). The additional peaks observed at 42.48˚ (111), 51.74˚ (200) and 72. 86˚ (220) are corresponding to elemental copper. Subsequently, the p-XRD pattern of MCW-Cu/Cu_2O-NS (Fig. 2. b) shows the characteristic peak at 2θ values of 42.33, 73.82 which are correspond to (111) and (220) planes of elemental copper respectively. Besides the copper peaks the additional peaks with high intensity (2θ = 29.49, 36.46, 61.49, 77.55) corresponding to (110), (111), (220), (222) planes of Cu_2O. All the observed peak values were consistent with the standard JCPDS No. 04-0836 for copper and 05-667 for Cu_2O with FCC crystal pattern [8–11, 18]. The obtained p-XRD pattern depicted the co-existence of two different crystal phase i.e. elemental copper and cuprous oxide. This demonstrates unequivocally that the oxidation process might produced the elemental Cu nanoparticels that underwent decomposition due to the copper and Cu_2O decreased stability during the bio reduction step. The peak broadening (MCW-Cu/Cu_2O-NS) in the p-XRD pattern indicates the presence of small nanostructures.

(Fig. 2)

3.3. FE-SEM analysis

The morphology of synthesized Cu/Cu_2O-NS samples was recorded by FE-SEM with different magnification (Figs. 3 & 4). The FE-SEM micrographs of TCW-Cu/Cu_2O-NS show the unique octahedral Cu_2O particles with Cu spherical particles distribution. The average edge length of these octahedral is measured to be about 250–300 nm. Figure 4 (a & b) displays the perfect spheres feature with diameters mainly ranging from 150–200 nm of Cu/Cu_2O-NS in heterogeneous form. The smooth surfaces of Cu/Cu_2O-NS could be observed by the high magnification (Fig. 3b & 4b) which could enlarge their contact area and then improve the utilization. The elemental compositions of the synthesized samples were further investigated by EDS (Energy Dispersive X-Ray Spectroscopy) and established the heterogeneity of the samples (Fig. 3c & 4c). Almost heterogeneous distribution of copper and cuprous oxide was observed in whole region with carbon and oxygen.

(Fig. 3) **&** (Fig. 4)

3.4. HR-TEM analysis

The HR-TEM images given in figure (5 & 6) illustrate the morphological characterization of synthesized samples. The TEM micrographs clearly depicted the mixed phases of copper and cuprous oxide (Fig. 5) in octahedral pattern with cubic symmetry, which is bounded by eight planes [45]. Anisotropic crystal growth rates that lead to non-spherical structures are assumed to be the primary cause of particle growth due to loss of surface enegy. In general, the process variables and inherent structure of nanoparticles play a major role in determining their morphology. It was discovered that the development rate varied along several crystallographic axes. The quickly expanding plan determines the final shape. As a result, Cu/Cu_2O-NS production may involve nucleation, selective adsorption and growth processes [46]. The

particle size and morphology of the Cu/Cu_2O-NS from TEM micrographs displays similarity to the results obtained by FE-SEM micrographs.

(Fig. 5) & (Fig. 6)

3.5. Zeta potential (ζ) Analysis

The Zeta potential (ζ) investigation is regarded as a significant parameter for the characterization of nanoparticles because it provides information about the stability of colloidal particles [11]. In addition, it has been established that zeta potential measurements of nanoparticles are required for biomedical applications [20]. In order to ascertain the materials' colloidal stability, the zeta (ζ) potentials of Cu/Cu_2O-NS were examined (Fig. 7). The obtained zeta (ζ) potential value for Cu/Cu_2O-NS is found to be – 30.28 mV and – 35.04 mV for TCW-Cu/Cu_2O-NS and MCW-Cu/Cu_2O-NS respectively. The derived zeta potential values are consistent with reported values [11, 13]. Additionally, high negative zeta potential (ζ) depends on the aggregation of particles and also indicates an enhanced double layer repulsion of nanoparticles [3]. This highlights the strong electrostatic repulsion and high degree of dispersion that the free electrons on the Cu/Cu_2O-NS surfaces with various bio-molecules present in TCW and MCW. It was proposed that the electrical charge of the copper nanoparticles enhance its biological properties [23]. A higher negative zeta potential is caused by the action of strong electrostatic repulsion between ultrafine particles, impending aggregation and agglomeration in liquid media, implying long term stability and quality of nanoparticles [22].

(Fig. 7)

3.6. Surface area analysis

The specific surface area (S_{BET}) and pore size distribution (PSD) of the synthesized samples were estimated by the nitrogen sorption isotherms. Figure 8 depicts a representative sorption isotherms and the corresponding pore distribution (inset of Fig. 8) of the samples. The obtained nanostructures demonstrated the type IV isotherms depicted the pore as mesopores and the hysteresis showed the H2 type B. The hysteresis loops are broad and the desorption curves are steeper than the adsorption curves, indicating different distributions of pore types and pore diameters in the samples. This is usually the case for slit pores and two parallel plate cracks [47]. The BET surface areas were measured as 53.25 $m^2 g^{-1}$ and 103.29 $m^2 g^{-1}$ for TCW-Cu/Cu_2O-NS and MCW-Cu/Cu_2O-NS (Table 1). The MCW-Cu/Cu_2O-NS shows a twofold area increase than TCW-Cu/Cu_2O-NS. According to the findings of SEM and HR-TEM, the MCW-Cu/Cu_2O-NS spheres have more pores that are open to N_2 molecules [48]. This can be explained by the mechanism of ion doping. That is, at higher salt concentrations, the rapid precipitation may increase the ion doping, resulting in more counter ions trapped inside. In that case, MCW-Cu/Cu_2O-NS has more defects and is highly porous. However, the TCW-Cu/Cu_2O-NS shows crystals with lesser or no defect, showing an ideal octahedral morphology and a thick solid without visible voids inside [49]. The pore volumes of Cu/Cu_2O-NS were determined by Barrett-Joyner- Halenda (BJH) adsorption method to be

0.068 cc g^{-1} and 0.158 cc g^{-1} for TCW-Cu/Cu_2O-NS and MCW-Cu/Cu_2O-NS. The maximum pore radius for TCW-Cu/Cu2O-NS and MCW-Cu/Cu_2O-NS is 37.0 Å and 36.5 Å respectively [50]. Other comparable nanostructured materials have a smaller surface area, according to recent investigations [51–53]. When comparing the results, it was found to that the current studies had a larger surface area and had more active sites, as shown by the BET surface area measurement and pore size distribution analysis. The synthesized MCW-Cu/Cu_2O-NS possessed a large specific surface area and correspondingly increased the number of the contact sites for living cells, which enhanced the adsorption of living cells [52, 54].

Table 1
Surface area and Pore size distributions of Cu/Cu_2O-NS

S. No.	Sample	BET Surface area (m^2/g)	Pore radius dV(r) (nm) BJH adsorption	Pore Volume (cc/g)	Total pore volume (nm) at $P/P_0 = 0.988$
1.	TCW-Cu/Cu_2O-NS	55.63	3.70	0.068	84.97
2.	MCW-Cu/Cu_2O-NS	103.92	3.65	0.158	79.55

(Fig. 8) & (Table 1)

3.7. Biological studies

3.7.1. Antibacterial activity

Antibacterial activities of synthesized Cu/Cu_2O-NS were assessed against both Gram + Ve and Gram – Ve bacteria. (Fig. 9 & Table S1). The MCW-Cu/Cu_2O-NS revealed potential antibacterial efficacy against Arthrobacter spp. (ZoI ~ 10 mm at the concentration 20 µg/ml, Fig. 9. b) whereas the TCW-Cu/Cu_2O-NS did not show any ZoI against Arthobacter spp (Fig. 9. a). TCW-Cu/Cu_2O-NS showed significant inhibition (4 mm at the concentration 20 µg/ml) against *E.coli* bacterial strain (Fig. 9.c), but there was no zone formed by MCW-Cu/Cu_2O-NS (Fig. 9. d). Bacterial strain *K. pneumonia* showed a zone of inhibition against TCW-Cu/Cu_2O-NS while it did not show a zone against MCW-Cu/Cu_2O-NS. These results indicating that the zone of inhibition was increased while the concentration of samples increased. The antibacterial activity of Cu_2O was reported as the contact of nanostructures with the surface of bacteria, which subsequently led to degradation and inactivation of bacteria [56]. This contact killing was broadly adopted by many researchers as a mechanism for the antibacterial activities of Cu_2O [55, 56].

(Fig. 9)

3.7.2. Assessment of Free radical scavenging ability of Cu/Cu_2O-NS

Antioxidants have been used as therapeutic agents because of their ability to possess anticancer, anti-inflammatory, anti-mutagenic, anticancer, antibacterial and anti-atherosclerotic characteristics [27, 58, 59]. Figure 10 shows the UV-Vis. spectral studies of DPPH free radical scavenging ability of Cu/Cu_2O-NS, the intensity of absorbance peak at 517 nm decreases with increase the concentration of Cu/Cu_2O-NS which attests the radical scavenging ability of Cu/Cu_2O-NS. The inhibitory concentration (IC_{50}) values were found to be 88.31 µg/ml, 27.26 µg/ml, for TCW-Cu/Cu_2O-NS and MCW-Cu/Cu_2O-NS (Fig. 10 inset). It reflects that Cu/Cu_2O-NS has the potential to transfer its electrons towards the free radicals present in nitrogen atom in DPPH [60]. Biosynthesized copper nanoparticles have been shown in numerous studies to have potent antioxidant action even at low concentrations [61–63].In is strongly encouraged to employ natural antioxidants for health protections in addition to lowering othr types of oxidative stress connected to degenerative illness. The results obtained validated the Cu/Cu_2O-NS extraordinarily high antioxidant activity. The odd electron is the cause of the radical scavenging of DPPH by Cu/Cu_2O-NS. DPPH exhibits a prominent absorption band at 517 nm in the visible spectrum, odd electron pairing off causes the diminishing absorbance when a free radical scavenger is present [64]. The DPPH is transformed into a $DPPH^-$ anion by accepting one electron from the Cu/Cu2O-NS, and it is then transformed into a DPPH-H by accepting one proton from the same substance. This indicated two stage processes for the DPPH scavenging reaction, with the first step absorbing electrons and the second step accepting protons [65].

(Fig. 10)

3.7.3. Anticancer Activity

3.7.3.1. Cytotoxicity (MTT assay)

The cytotoxicty profile of Cu/Cu_2O-NS was given in Fig. 11 (A) & 12 (A.). The concentration dependent curves of the Cu/Cu_2O-NS illustrated the promising cytotoxicity on booth lung and cervical cancer cell lines. Among two samples, MCW-Cu/Cu_2O-NS revealed commendable activity against both cancer cell lines. The samples exhibited IC_{50} values around half of the standard drug cisplatin and results have been given in table (2). The IC_{50} values of TCW-Cu/Cu_2O-NS and MCW-Cu/Cu_2O-NS against HeLa cell line, the IC_{50} values were determined as 28 ± 0.7 µg/ml and 23 ± 1.2 µg/ml, whereas against HeLa cell linem the IC_{50} values were 26 ± 1.2 µg/ml and 20 ± 1.5 µg/ml respectively. The Cu/Cu_2O-NS instigate various morphological alterations against A549 cells and HeLa cells at 48 hr incubation; though there were no such changes were seen in untreated cells (Fig. 11. B (a); 12. B (a)). The cytotoxicity of Cu/Cu_2O-NS might be because of the penetration of metal ions into the cellular components, which in turn, led to the production of ROS, increasing oxidative stress leading to apoptotic cell death. The damage of cellular

protein functioning enzyme such as protein kinases was reported to be, by the interface complex of nanostructures and cellular components [66].

(Fig. 11) (Fig. 12) (Table 2)

Table 2
Cytotoxicity of Cu/Cu_2O-NS (µg/ml) against Cancer Cell Lines (IC_{50}):

S. No	Sample	Cell lines	
		A549	HeLa
1.	Cisplatin (Standard)	14 ± 1.7	15 ± 1.5
2.	TCW-Cu/Cu_2O-NS	28 ± 0.7	26 ± 1.2
3.	MCW-Cu/Cu_2O-NS	23 ± 1.2	20 ± 1.5

3.7.3.2. Apoptosis Assessment (AO/EB staining assay)

Anti-proliferative effects of Cu/Cu_2O-NS on A549 and HeLa cell lines were studied by AO/EB staining assay (Figs. 13 & 14). The samples exposed A549 and HeLa cells showed some changes in their cell shape, whereas untreated control cells did not show any such changes. The degree of apoptosis instigate is crucial for the formation of anticancer medications [21]. Using fluorescence microscope, the morphology of necrotic, apoptotic and normal cells of A549 and HeLa cells were identified after staining with AO/EB and based on the integrity of the cell membrane. The control/untreated A549 and HeLa cells (Fig. 13 (a) & Fig. 14 (a)) showed green fluorescence expressing the existence of viable cells. The rate of apoptotic cells was calculated using the corresponding control cells after Cu/Cu_2O-NS treatment. In the two cell lines, orange apoptotic cells showing the occurrence of apoptosis and red necrotic cells were seen in figures (Figs. 13 (b, c, d) & 14 (b, c, d). However, due to the loss of cell membrane integrity brought on by Cu/Cu_2O-NS induced cytotoxicity. Interestingly, MCW-Cu/Cu_2O-NS treated cells had more apoptotic bodies than TCW-Cu/Cu_2O-NS treated cells

(Fig. 13) & (Fig. 14)

3.7.3.3. Cell cycle analysis (FACS)

The cell cycle defines the series of events that takes place in a cell as it grows and divides. The interruption of the cancer cells control over their cell cycle, which inhibits cell proliferation, may be one the anticancer drugs' modes of action. The cytotoxicity of Cu/Cu_2O-NS was analyzed using phase contrast microscopic observations (Figs. 11 & 12) and the apoptotic cell death by AO/EB stained fluorescence (Figs. 13 & 14) microscopic analysis. In order to ascertain the cell death mechanism, flow cytometry was used which employed in A549 cells treatment with MCW-Cu/Cu_2O-NS. Figure 15 (a-d) shows the DNA count in untreated and MCW-Cu/Cu_2O-NS treated A549 cells evaluated at 24 hr incubation and the rate of

cell mortality was reckoned. Comparing the DNA counts for the G0/G1, S, and Gr/M phases, it was shown that the S phase in A549 cells had high cell mortality rate. Whereas in G2/M phase, a similar inclination to degrade DNA counts is found in DNA count in untreated A549 cells was 27.31% in S phase and subsequently decreased to 18.72% with MCW-Cu/Cu2O-NS treatment at 50 µg/ml.

(Fig. 15)

4. Conclusion

Novel heterogeneous architecture of Cu/Cu_2O-NS was successfully synthesized with octahedral and spherical nanostructures. In order to confirm the existence of copper and cuprous oxide, the obtained nanostructures were analyzed by various physicochemical techniques. The present work mainly focused on the biological properties of coconut water mediated Cu/Cu_2O-NS. Taken together, this current work clearly authoritative that the potential antibacterial, antioxidant and anticancer activity of both TCW-Cu/Cu_2O-NS and MCW-Cu/Cu_2O-NS. These nanostructures have many biomedical applications and could be efficiently used as drug carrier. Hence, the novel heterogeneous Cu/Cu_2O-NS may become a potential candidate for the establishment of promising biomedical agent.

Declarations

Acknowledgement

We are thankfully acknowledge UGC, New Delhi and TANSCHE, Chennai for financial assistants in the form of UGC major Research Project (File No: 39-724/2010 (SR); Dated 11-01-2011); & TANSCHE minor research project scheme (Rc. No. 2026/2020A, Dt. 01.02.2021). We thank our former principal Dr. V. KALAISELVI, Dr. K. CHITRA (former principal), Govt. Arts College (Autonomous), Coimbatore – 641 018, for their constant encouragement and valuable discussions. We do extend our warm gratitude to Dr. M. PAULPANDI, Department of Proteomics, Bharathiar University, Coimbatore – 641 046 for his help in carrying out certain biological studies.

Ethical Approval: Not Applicable.

Funding: We are thankfully acknowledging (1). University Grants Commission (UGC), New Delhi for financial assistant (given to Dr. A.R.) in the form of UGC Major Research Project (File No: 39-724/2010 (SR); Dated 11-01-2011); and Tamil Nadu State Council for Higher Education (TANSCHE), Chennai for Minor Research Project Scheme to Dr. A.R. (Rc. No. 2026/2020A, Dt. 01.02.2021).

Availability of Data and Materials:

The data that support the findings of this study are available and the same can be accessed at any time on request from one of the Corresponding Authors [Dr. A. R].

Conflict of Interest: The Authors claim no conflicts of interest.

References

1. S.S. Skeeters, A.C. Rosu, Divyanshi, J. Yang, K. Zhang, ACS Appl. Mater. Interfaces, 12, 50203 (2020). https://doi.org/10.1021/acsami.0c11052.
2. Y. Yan, C. Li, H. Wu, J. Du, J. Feng, J. Zhang, L. Huang, S. Tan, Q. Shi, ACS Appl. Bio Mater. 2, 1842 (2019). https://doi.org/10.1021/acsabm.8b00695.
3. M.J. Woźniak-Budych, Ł. Przysiecka, B.M. Maciejewska, D. Wieczorek, K. Staszak, M. Jarek, T. Jesionowski, S. Jurga, ACS Biomater. Sci. Eng. 3, 3183 (2017). https://doi.org/10.1021/acsbiomaterials.7b00465.
4. M.S. Bhalerao, A.V. Patwardhan, M.A. Bhosale, V.M. Kulkarni, B.M. Bhanage, RSC Adv. 6, 38906 (2016). https://doi.org/10.1039/C6RA00588H
5. H. Li, Z. Su, S. Hu, Y. Yan, Appl. Catal. B: Environ. 207, 134 (2017). https://doi.org/10.1016/j.apcatb.2017.02.013.
6. S. Thoka, A.-T. Lee, M.H. Huang, ACS Sustainable Chem. Eng. 7, 10467 (2019). https://doi.org/10.1021/acssuschemeng.9b00844.
7. H. Huang, J. Zhang, L. Jiang, Z. Zang, J. Alloys Compd. 718, 112 (2017). https://doi.org/10.1016/j.jallcom.2017.05.132
8. N. Li, W. Yan, Y. Niu, S. Qu, P. Zuo, H. Bai, N. Zhao, ACS Appl. Mater. Interfaces, 13, 9838 (2021). https://doi.org/10.1021/acsami.0c20636.
9. K. Giannousi, G. Sarafidis, S. Mourdikoudis, A. Pantazaki, C. Dendrinou-Samara, Inorg. Chem. 53, 9657 (2014). https://doi.org/10.1021/ic501143z.
10. W. Zhou, L. Fu, L. Zhao, X. Xu, W. Li, M. Wen, Q. Wu, ACS Appl. Mater. Interfaces, 13, 10878 (2021). https://doi.org/10.1021/acsami.0c21336.
11. A. Tegenaw, G.A. Sorial, E. Sahle-Demessie, C. Han, Environ. Pollut. 253, 278(2019). https://doi.org/10.1016/j.envpol.2019.07.036.
12. M. Zhou, M. Tian, C. Li, Bioconjug. Chem. 27, 1188 (2016). https://doi.org/10.1021/acs.bioconjchem.6b00156
13. M. Sriramulu, S. Shanmugam, V.K. Ponnusamy, Colloid Interface Sci. Commun. 35, 100254 (2020). https://doi.org/10.1016/j.colcom.2020.100254
14. X. Luo, C. Li, D. Yang, F. Liu, Y. Chen, Mater. Chem. Phys. 151, 252 (2015). https://doi.org/10.1016/j.matchemphys 2014.11.062
15. A.-J. Wang, J.-J. Feng, Z.-H. Li, Q.-C. Liao, Z.-Z. Wang, J.-R. Chen, Solvothermal synthesis of Cu/Cu_2O hollow microspheres for non-enzymatic amperometric glucose sensing, Cryst. Eng. Comm. 14, 1289 (2012). https://doi.org/10.1039/C1CE05869J
16. D. Rehnlund, M. Valvo, C.-W. Tai, J. Ångström, M. Sahlberg, K. Edström, L. Nyholm, Nanoscale, 7, 13591 (2015). https://doi.org/10.1039/C5NR03472H

17. W. Wei, Y. Lu, W. Chen, S. Chen, J. Am. Chem. Soc. 133, 2060 (2011). https://doi.org/10.1021/ja109303z
18. X. Xu, K. Jia, S. Chen, D. Lang, C. Yang, L. Wang, R. Wu, W. Wang, J. Wang, J. Environ. Chem. Eng. 9, 105505 (2021). https://doi.org/10.1016/j.jece.2021.105505
19. O. L. Evdokimova, M.E. Belousova, A.V. Evdokimova, T.V. Kusova, A.E. Baranchikov, K.S. Antonets, A.A. Nizhnikov, A.V. Agafonov, Cellulose, 28, 2931 (2021). https://doi.org/10.1007/s10570-021-03689-x
20. I. Jahan, F. Erci, I. Isildak, J. Drug Deliv. Sci. Technol. 61, 102172 (2021). https://doi.org/10.1016/j.jddst.2020.102172
21. U. Jinu, M. Gomathi, I. Saiqa, N. Geetha, G. Benelli, P. Venkatachalam, Microb. Pathog. 105, 86 (2017). https://doi.org/10.1016/j.micpath.2017.02.019
22. H. Ashraf, T. Anjum, S. Riaz, I.S. Ahmad, J. Irudayaraj, S. Javed, U. Qaiser, S. Naseem, Nano, 8, 1729 (2021). https://doi.org/10.1039/D0EN01281E
23. S.C. Mali, A. Dhaka, C.K. Githala, R. Trivedi, Biotechnol. Rep. 27, e00518 (2020). https://doi.org/10.1016/j.btre.2020.e00518
24. S.S. Biresaw, P. Taneja, Mater. Today: Proc. 49, 3501 (2022). https://doi.org/10.1016/j.matpr.2021.07.149
25. A. Chinnathambi, T. Awad Alahmadi, S. Ali Alharbi, Artif. Cells, Nanomed. Biotechnol. 49, 500 (2021). https://doi.org/10.1080/21691401.2021.1926275.
26. Z. Dashtizadeh, F. Jookar Kashi, M. Ashrafı, Mater. Today Commun. 27, 102456 (2021). https://doi.org/10.1016/j.mtcomm.2021.102456
27. B. Djamila, L.S. Eddine, B. Abderrhmane, A. Nassiba, A. Barhoum, Biomass Conv. Bio ref. (2022). https://doi.org/10.1007/s13399-022-02743-3.
28. S. Torres-Arellano, O. Reyes-Vallejo, J. Pantoja Enriquez, J.L. Aleman-Ramirez, A.M. Huerta-Flores, J. Moreira, J. Muñiz, L. Vargas-Estrada, P.J. Sebastian, Fuel, 285, 119152 (2021). https://doi.org/10.1016/j.fuel.2020.119152
29. M.F. Al-Hakkani, S.H.A. Hassan, M.S. Saddik, M.A. El-Mokhtar, S.A. Al-Shelkamy, J. Mater. Res. Technol. 14, 1998 (2021). https://doi.org/10.1016/j.jmrt.2021.07.076
30. S. Sampaio, J.C. Viana, Mater. Sci. Eng.: B, 263, 114807 (2021). https://doi.org/10.1016/j.mseb.2020.114807
31. K. Manna, A. Khan, D. Kr. Das, S. Bandhu Kesh, U. Das, S. Ghosh, R. Sharma Dey, K. Das Saha, A. Chakraborty, S. Chattopadhyay, S. Dey, D. Chattopadhyay, J. Ethnopharmacol, 155, 132 (2014). https://doi.org/10.1016/j.jep.2014.04.046.
32. S.K. Mantena, Jagadish, S.R. Badduri, K.B. Siripurapu, M.K. Unnikrishnan, Food / Nahrung, 47, 126 (2003). https://doi.org/10.1002/food.200390023
33. P.P. Preetha, V.G. Devi, T. Rajamohan, Food Funct. 3, 753 (2012). https://doi.org/10.1039/C2FO30066D

34. R.R. Silva, D.O. e Silva, H.R. Fontes, C.S. Alviano, P.D. Fernandes, D.S. Alviano, Altern. Med. 13, 107(2013). https://doi.org/10.1186/1472-6882-13-107
35. M. DebMandal, S. Mandal, Coconut (Cocos nucifera L.: Arecaceae): Asian Pac. J. Trop. Med. 4, 241 (2011). https://doi.org/10.1016/S1995-7645(11)60078-3
36. P. Makvandi, C.-y. Wang, E.N. Zare, A. Borzacchiello, L.-n. Niu, F.R. Tay, Adv. Funct. Mater. 30, 1910021 (2020). https://doi.org/10.1002/adfm.201910021
37. S. Noor, Z. Shah, A. Javed, A. Ali, S.B. Hussain, S. Zafar, H. Ali, S.A. Muhammad, J. Microbiol. Methods, 174, 105966 (2020). https://doi.org/10.1016/j.mimet.2020.105966
38. A. Yaqub, N. Malkani, A. Shabbir, S.A. Ditta, F. Tanvir, S. Ali, M. Naz, S.A.R. Kazmi, R. Ullah, Curr. Microbiol. 77, 2287 (2020). https://doi.org/10.1007/s00284-020-02058-4
39. W.-H. Ke, C.-F. Hsia, Y.-J. Chen, M.H. Huang, Small, 12, 3530 (2016). https://doi.org/10.1002/smll.201600064
40. C.-F. Hsia, C.-H. Chang, M.H. Huang, Part. Part. Syst. Charact. 35, 1800112 (2018). https://doi.org/10.1002/ppsc.201800112
41. M.S. Aguilar, G. Rosas, J. Solid State Chem. 270, 192 (2019). https://doi.org/10.1016/j.jssc.2018.11.019
42. T.G. Hörner, P. Klüfers, Eur. J. Inorg. Chem. 2016, 1798 (2016). https://doi.org/10.1002/ejic.201600168
43. C.P. Ekasari, S. Widyarti, IOP Conf. Ser.: Earth Environ. Sci. 391, 012021 (2019). https://doi.org/10.1088/1755-1315/391/1/012021.
44. A. Samide, B. Tutunaru, Electroanalysis, 29, 2498 (2017). https://doi.org/10.1002/elan.201700281
45. D. Wang, Y. Wu, Z. Bai, J. Mater. Sci. 48, 7696 (2013). https://doi.org/10.1007/s10853-013-7589-x
46. S. Guo, Y. Fang, S. Dong, E. Wang, Inorg. Chem. 46, 9537 (2007). https://doi.org/10.1021/ic7016193
47. Y. Zhang, D. Shao, J. Yan, X. Jia, Y. Li, P. Yu, T. Zhang, J. Nat. Gas Geosci. 1, 213 (2016). https://doi.org/10.1016/j.jnggs.2016.08.002
48. B.M. Abu-Zied, M.A. Hussein, A. Khan, A.M. Asiri, Mater. Chem. Phys. 213, 168 (2018). https://doi.org/10.1016/j.matchemphys.2018.04.036
49. X. Song, W. Xu, D. Su, J. Tang, X. Liu, ACS Omega, 5, 1879 (2020). https://doi.org/10.1021/acsomega.9b03380.
50. X. Zhao, Y. Tan, F. Wu, H. Niu, Z. Tang, Y. Cai, J.P. Giesy, Sci. Total Environ. 571, 380 (2016). https://doi.org/10.1016/j.scitotenv.2016.05.151.
51. J. Li, L. Huang, X. Jiang, L. Zhang, X. Sun, Chem. Eng. J. 404, 127091 (2021). https://doi.org/10.1016/j.cej.2020.127091
52. M. Pandey, M. Singh, K. Wasnik, S. Gupta, S. Patra, P.S. Gupta, D. Pareek, N.S.N. Chaitanya, S. Maity, A.B.M. Reddy, R. Tilak, P. Paik, ACS Omega, 6, 31615 (2021). https://doi.org/10.1021/acsomega.1c04139.

53. D. Kichukova, I. Spassova, A. Kostadinova, A. Staneva, D. Kovacheva, Nanomaterials, 12, 2096 (2022). https://doi.org/10.3390/nano12122096
54. H.-f. Chen, J.-j. Wu, M.-y. Wu, H. Jia, New Carbon Mater. 34, 382 (2019). https://doi.org/10.1016/S1872-5805(19)30023-X.
55. L. Xiong, H. Yu, C. Nie, Y. Xiao, Q. Zeng, G. Wang, B. Wang, H. Lv, Q. Li, S. Chen, RSC Adv. 7, 51822 (2017). https://doi.org/10.1039/C7RA10605J
56. K. Sunada, M. Minoshima, K. Hashimoto, J. Hazard. Mater. 235-236, 265 (2012). https://doi.org/10.1016/j.jhazmat.2012.07.052
57. S. Meghana, P. Kabra, S. Chakraborty, N. Padmavathy, RSC Adv. 5, 12293 (2015). https://doi.org/10.1039/C4RA12163E
58. J. Kim, H. Park, G. Saravanakumar, W. J. Kim, ACS Appl. Mater. Interfaces, 13, 9390, (2020). https://doi.org/10.1021/acsami.0c15727
59. M. Hasanin, M.A. Al Abboud, M.M. Alawlaqi, T.M. Abdelghany, A.H. Hashem, Biol. Trace Elem. Res. (2021). https://doi.org/10.1007/s12011-021-02812-0
60. D. Das, B.C. Nath, P. Phukon, S.K. Dolui, Colloids Surf. B: Biointerfaces, 101, 430 (2013). https://doi.org/10.1016/j.colsurfb.2012.07.002
61. S. Wu, S. Rajeshkumar, M. Madasamy, V. Mahendran, Artif. Cells, Nanomed. Biotechnol. 48, 1153 (2020). https://doi.org/10.1080/21691401.2020.1817053
62. A. Muthuvel, M. Jothibas, C. Manoharan, Nanotechnol. Environ. Eng. 5, 14 (2020). https://doi.org/10.1007/s41204-020-00078-w
63. A. Velidandi, N.P.P. Pabbathi, S. Dahariya, R.R. Baadhe, Colloid Interface Sci. Commun. 38, 100302 (2020). https://doi.org/10.1016/j.colcom.2020.100302
64. S.S. Paul, M. Selim, A. Saha, K.K. Mukherjea, Dalton Trans. 43, 2835 (2014). https://doi.org/10.1039/C3DT52434E
65. L. Tabrizi, D.Q. Dao, T.A. Vu, RSC Adv. 9, 3320 (2019). https://doi.org/10.1039/C8RA09763A
66. T.I. Shaheen, A. Fouda, S.S. Salem, Ind. Eng. Chem. Res. 60, 1553 (2021). https://doi.org/10.1021/acs.iecr.0c04880

Schemes

Scheme 1 is available in the Supplementary Files section

Figures

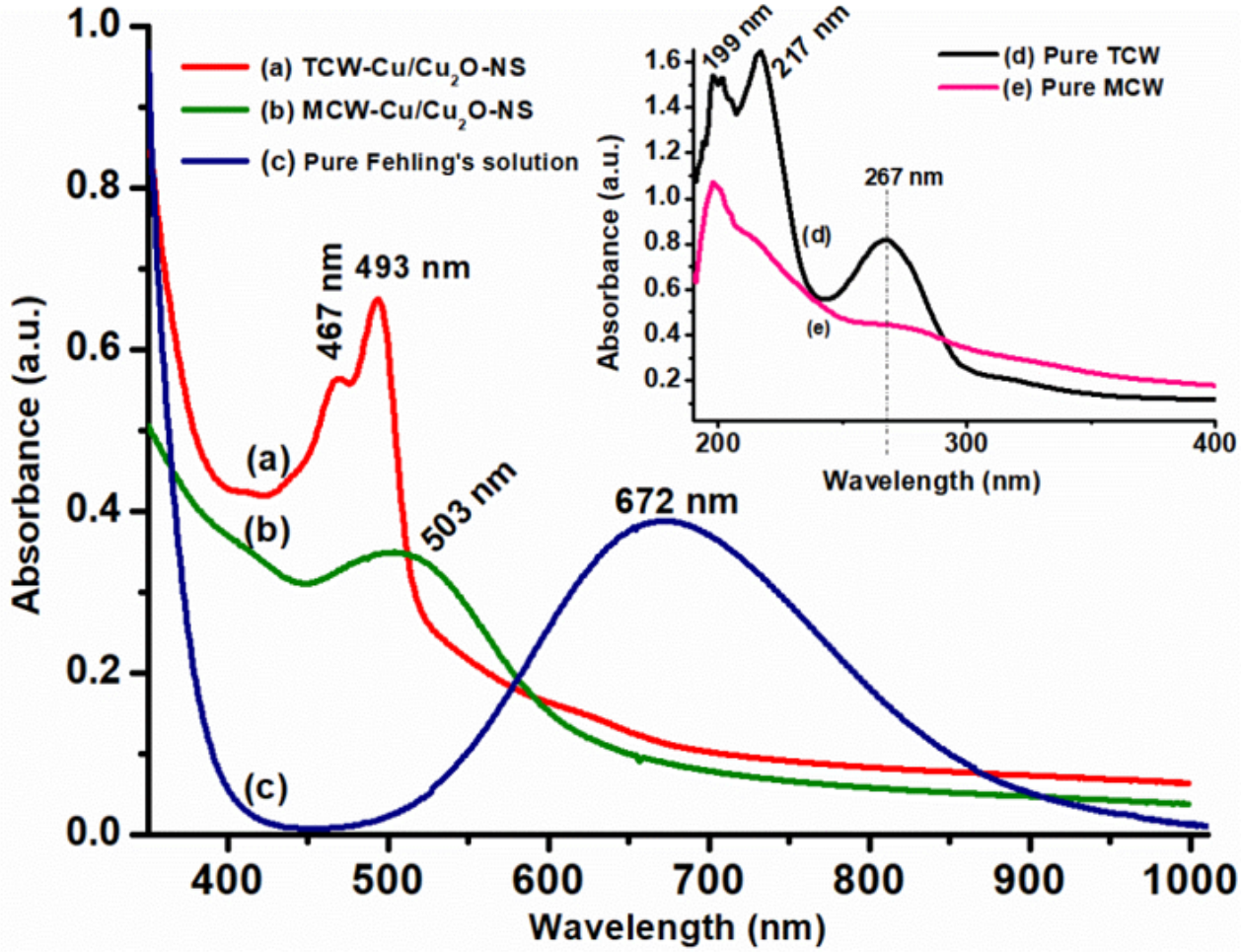

Figure 1

Figure 1

UV-Vis. Spectra of (a) TCW-Cu/Cu_2O-NS, (b) MCW-Cu/Cu_2O-NS, (c) Fehling's Solution, [(d) Tender coconut water (TCW), (e) Matured coconut water (MCW) (inset)]

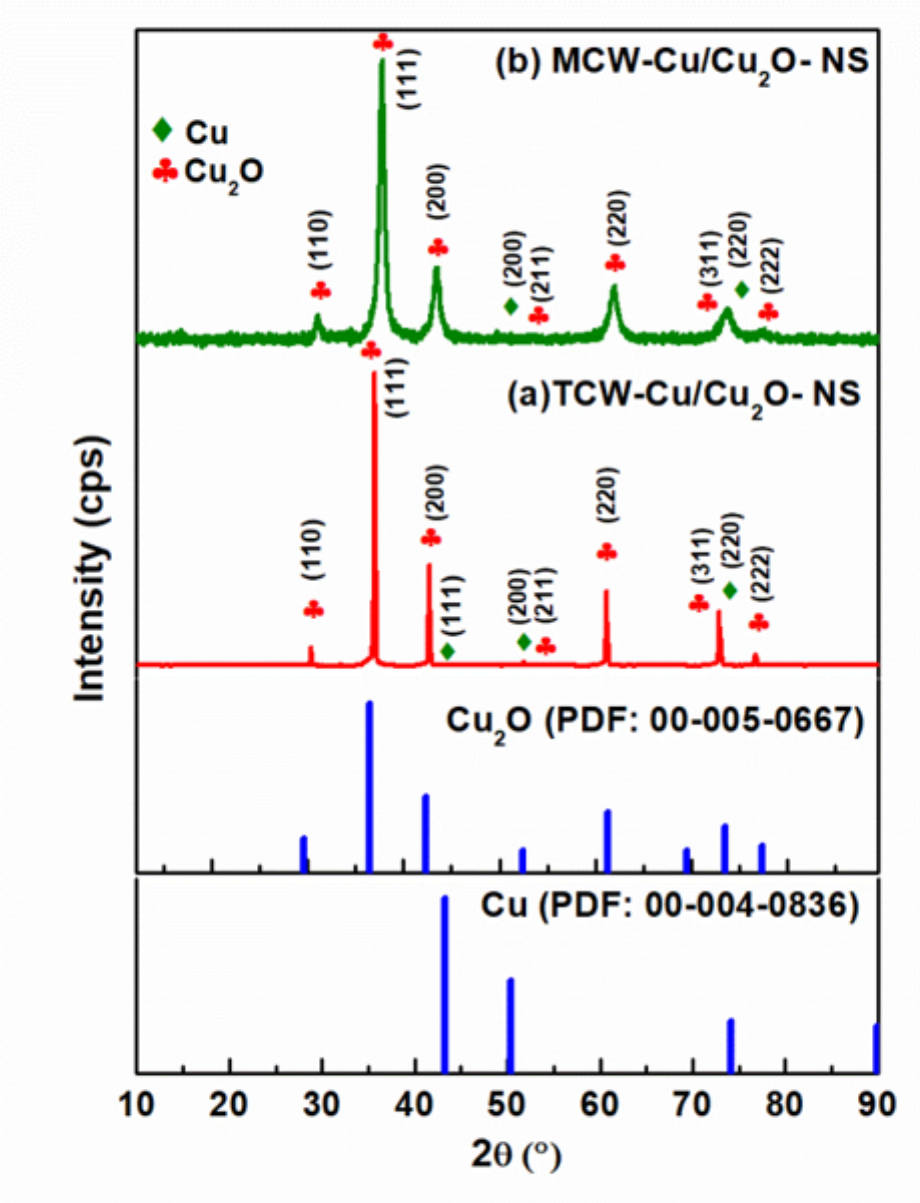

Figure 2

Figure 2

Powder XRD Pattern of (a) TCW-Cu/Cu_2O-NS and (b) MCW-Cu/Cu_2O-NS with corresponding JCPDS card.

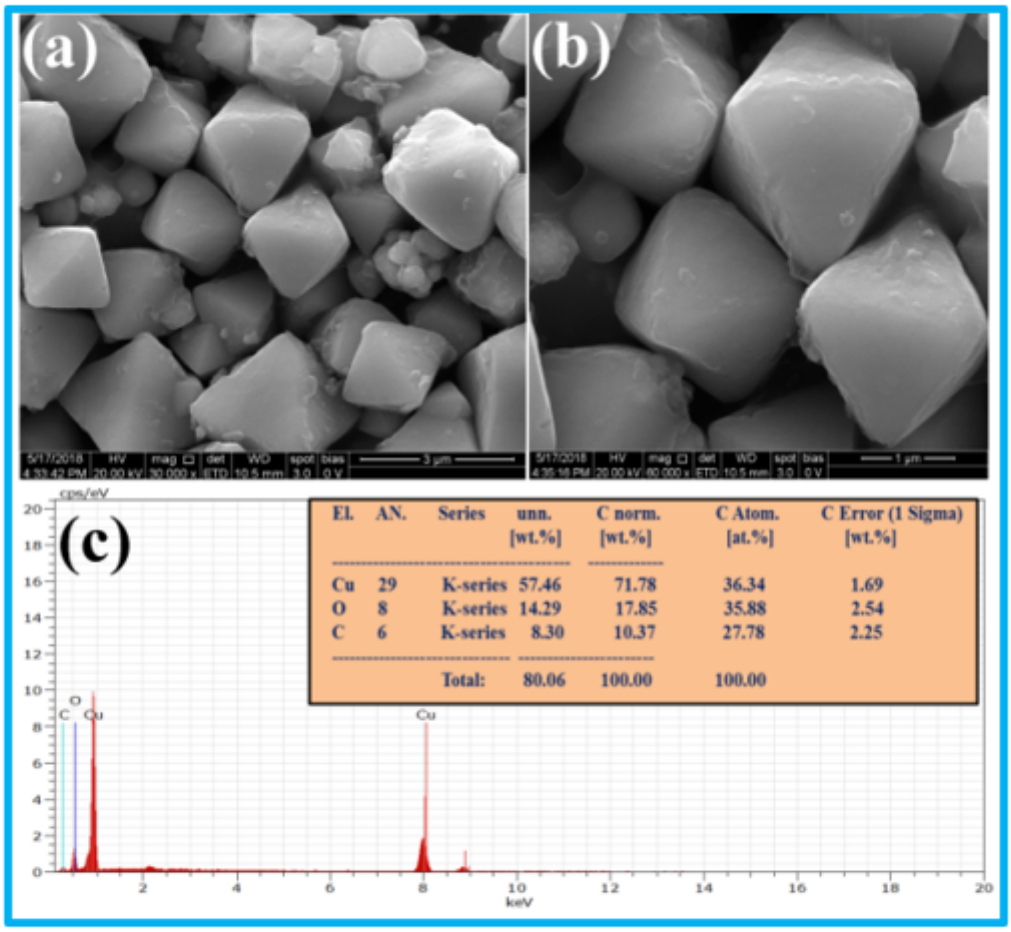

Figure 3

Figure 3

SEM images of TCW-Cu/Cu_2O-NS (a, b) and EDX spectrum (c)

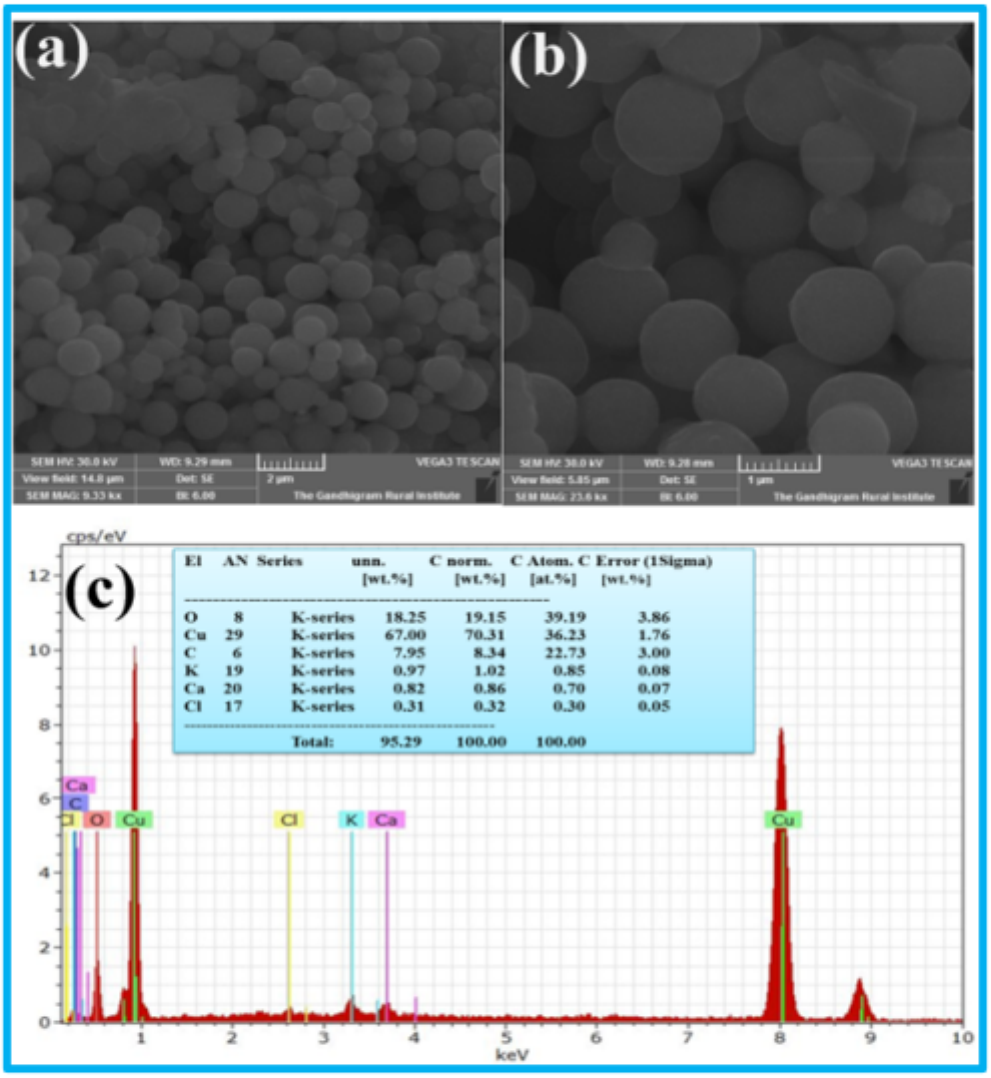

Figure 4

Figure 4

SEM images of MCW-Cu/Cu_2O-NS (a, b) and EDX spectrum (c)

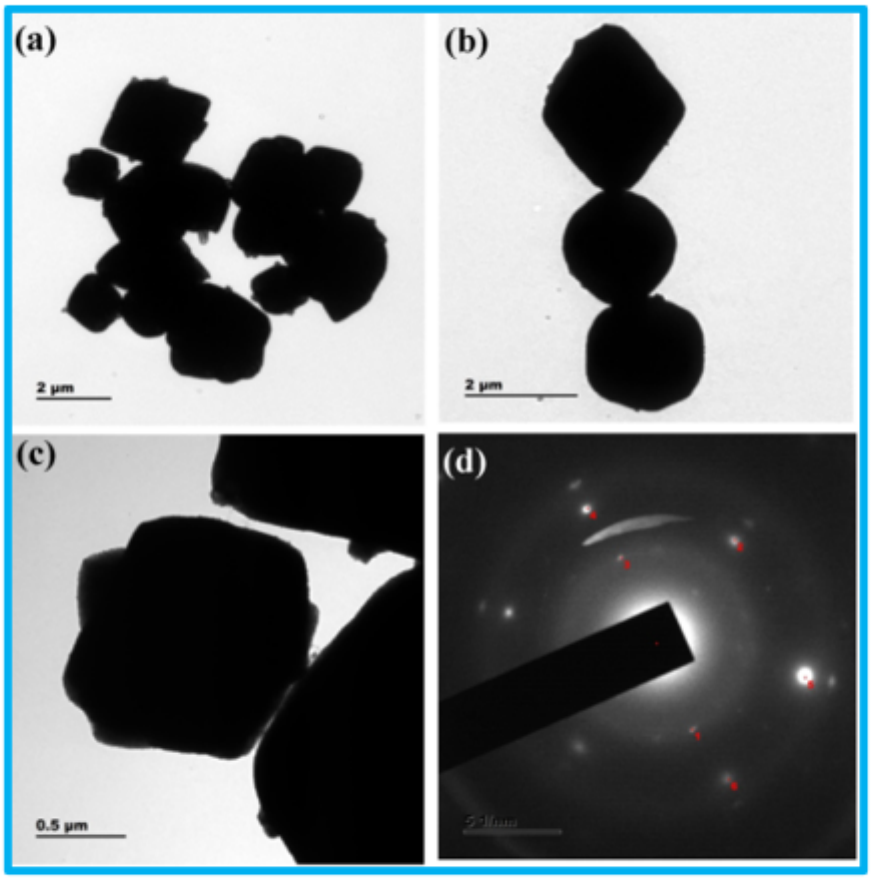

Figure 5

Figure 5

HR-TEM images of TCW-Cu/Cu_2O-NS (a, b, c) and SAED pattern (d)

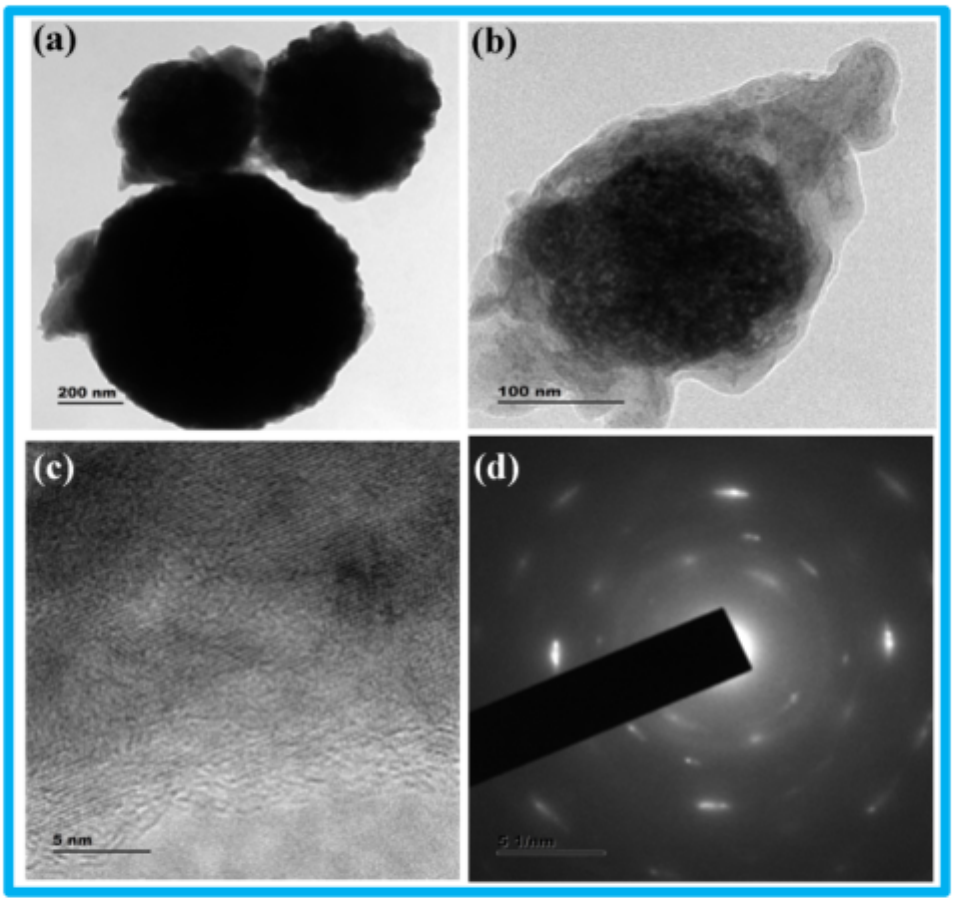

Figure 6

Figure 6

HR-TEM images of MCW-Cu/Cu_2O-NS (a, b), Lattice fringes (c) and SAED pattern (d)

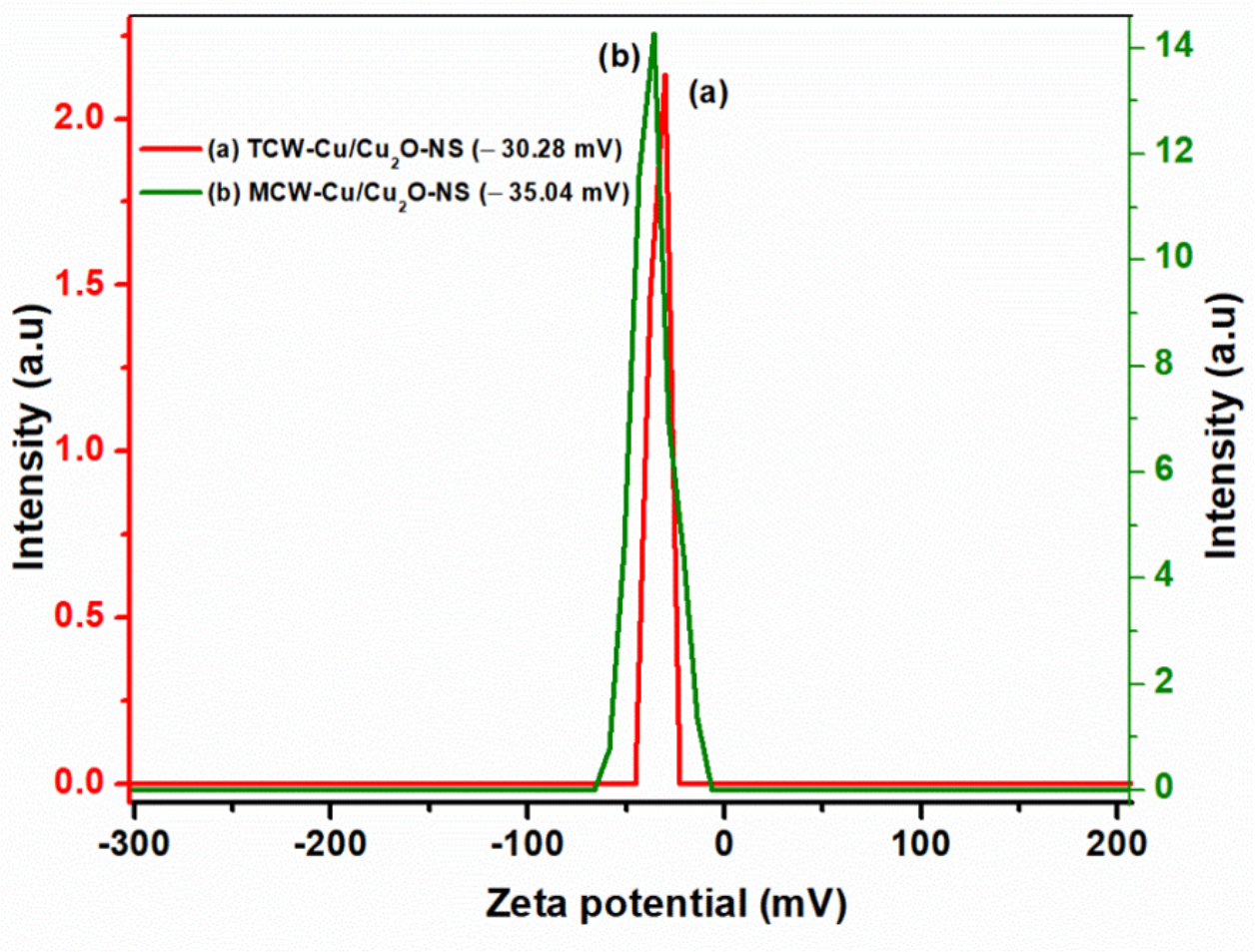

Figure 7

Figure 7

Zeta potential analysis of (a) TCW-Cu/Cu_2O-NS; and (b) MCW-Cu/Cu_2O-NS

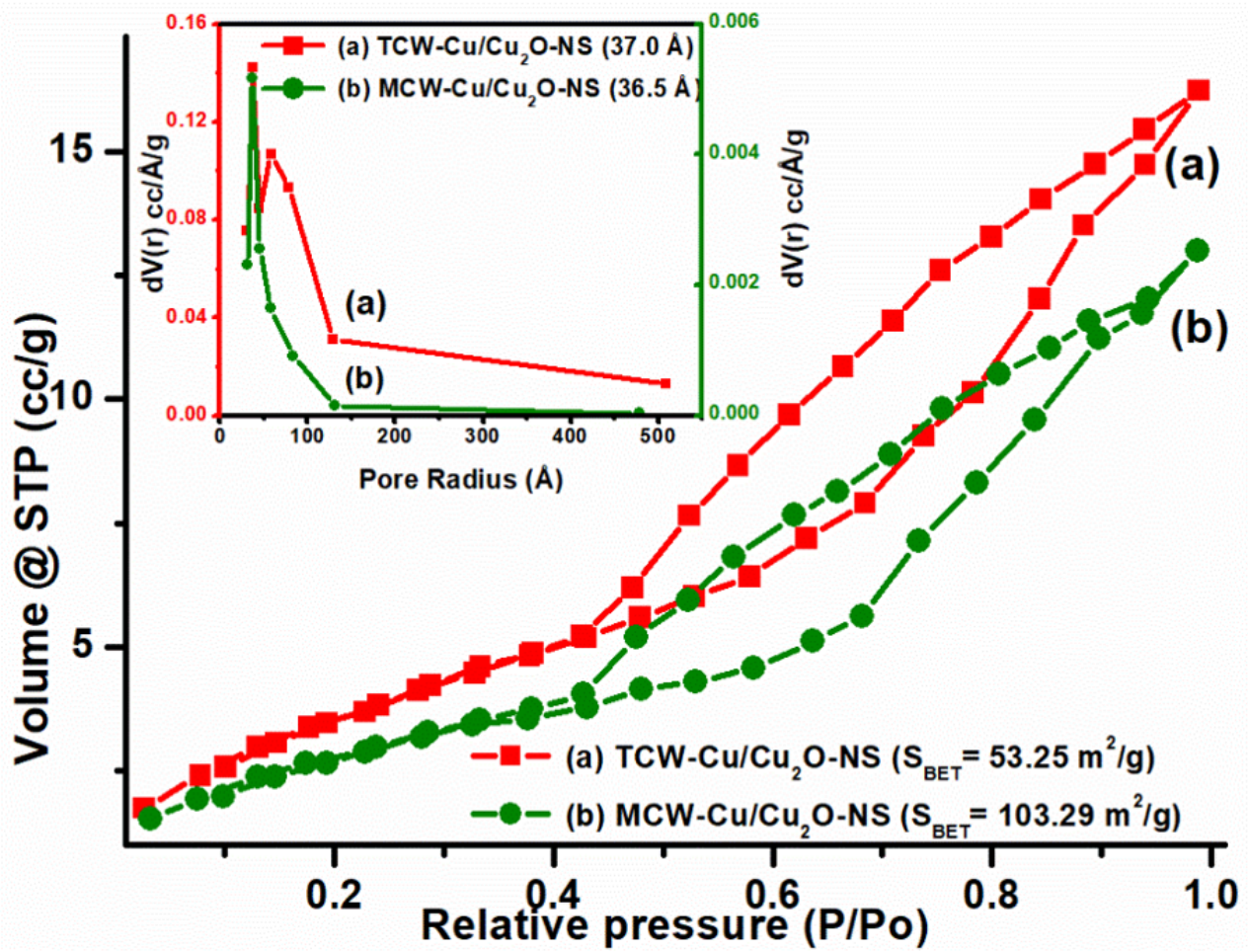

Figure 8

Figure 8

N_2 sorption isotherms and the corresponding pore size distribution (inset) of (a) TCW-Cu/Cu_2O-NS; (b) MCW-Cu/Cu_2O-NS

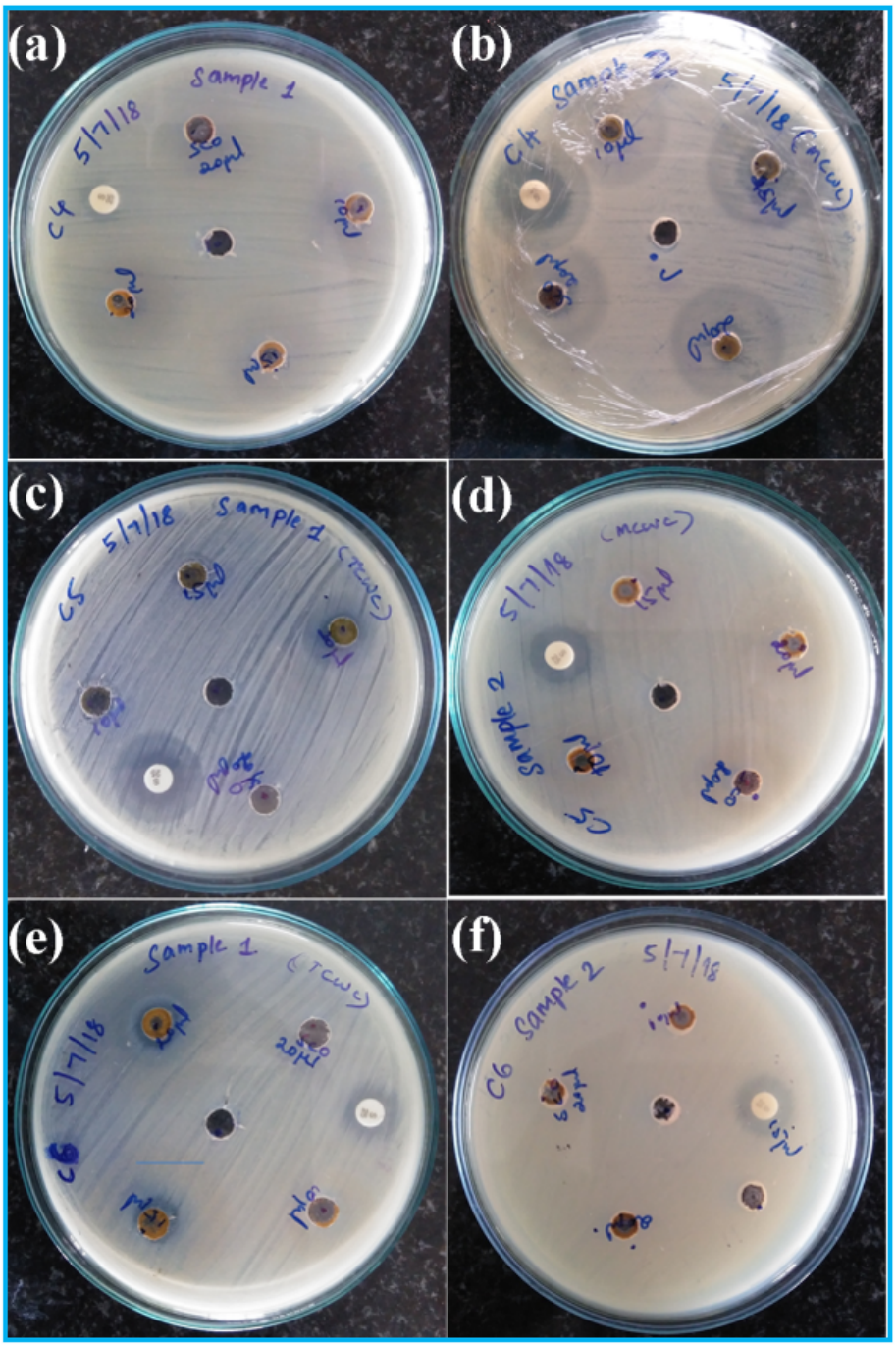

Figure 9

Figure 9

Anti-bacterial activity of TCW-Cu/Cu_2O-NS (a, c, e) and MCW-Cu/Cu_2O-NS (b, d, and f) against *Arthrobacter spp.*, *E. coli*, *K. pneumonia* respectively.

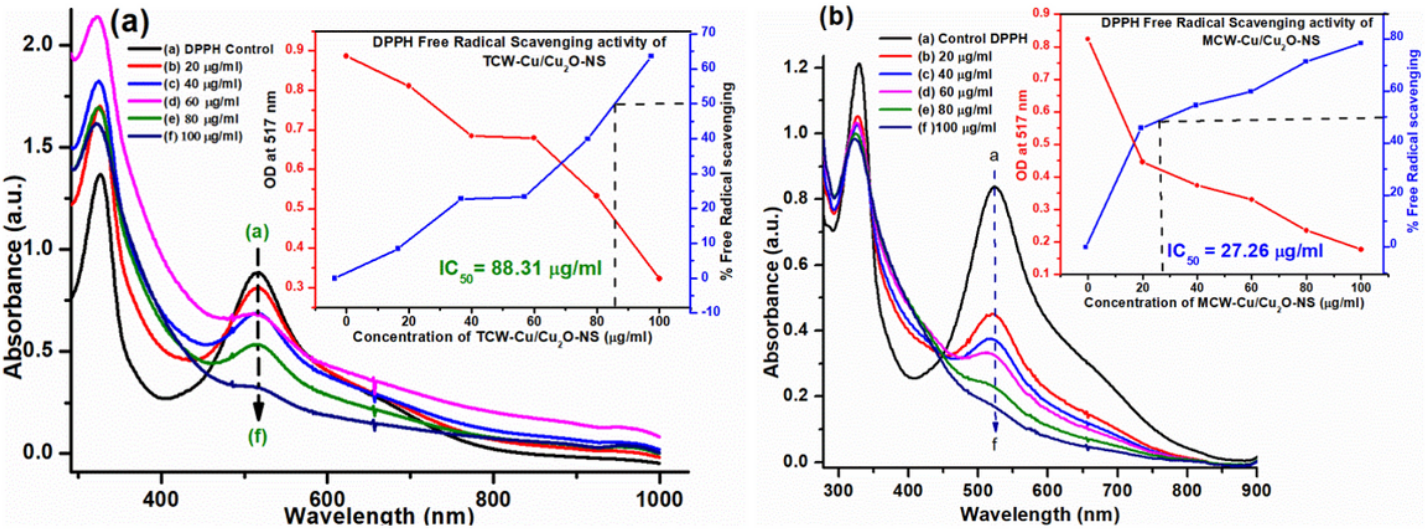

Figure 10

Figure 10

DPPH Radical Scavenging activities of (a) TCW-Cu/Cu_2O-NS (b) MCW-Cu/Cu_2O-NS

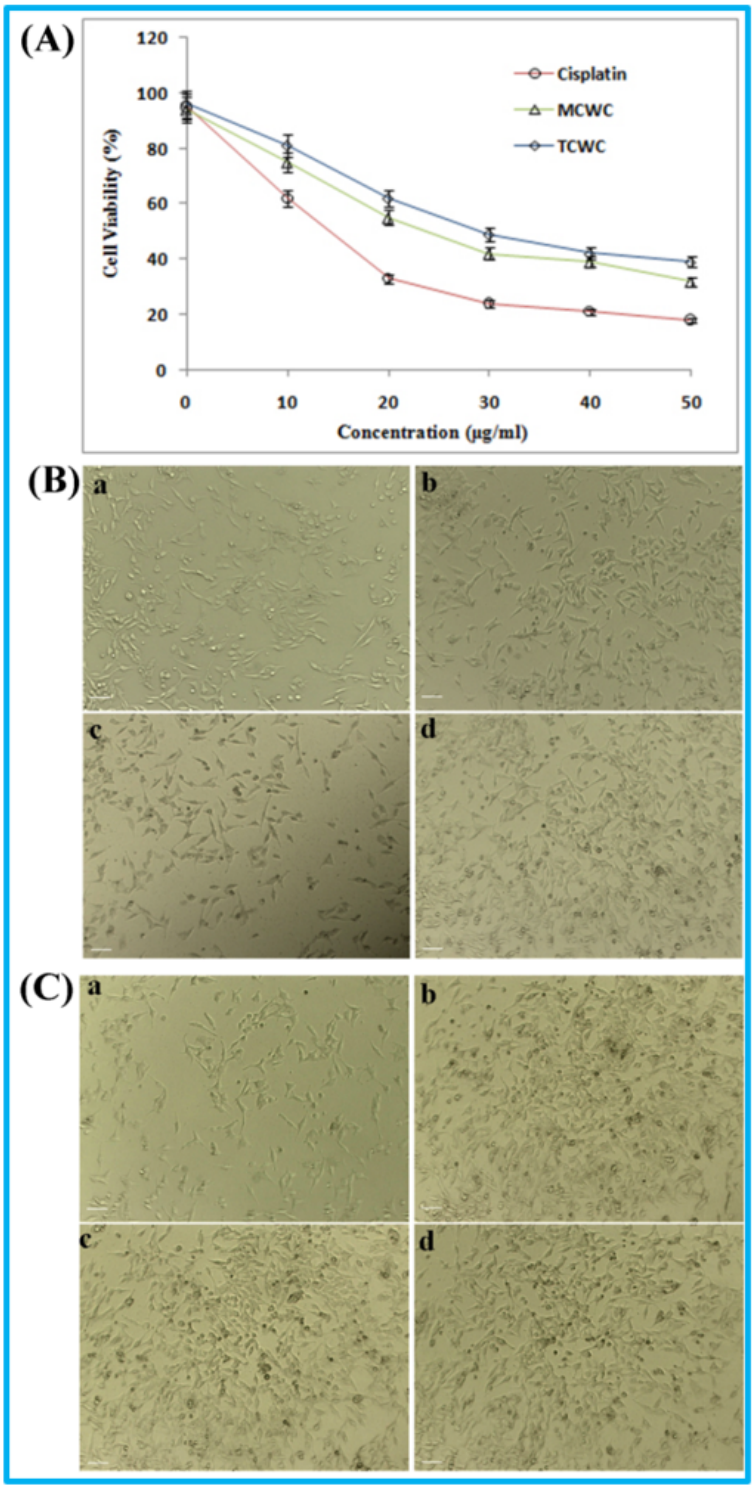

Figure 11

Figure 11

(A) Cytotoxicity in A549 cells treated with TCW-Cu/Cu_2O-NS, MCW-Cu/Cu_2O-NS and positive control Cisplatin (standard drug); (B) Phase contrast microscopic images of A549 cells (a) control (untreated) (b) 10 µg/ml, (b) 25 µg/ml, (c) 50 µg/ml treated with TCW-Cu/Cu_2O-NS;(C) Phase contrast microscopic images of A549 cells (a) control (untreated) (b) 10 µg/ml, (c) 25 µg/ml, (d) 50 µg/ml treated with MCW-Cu/Cu_2O-NS .

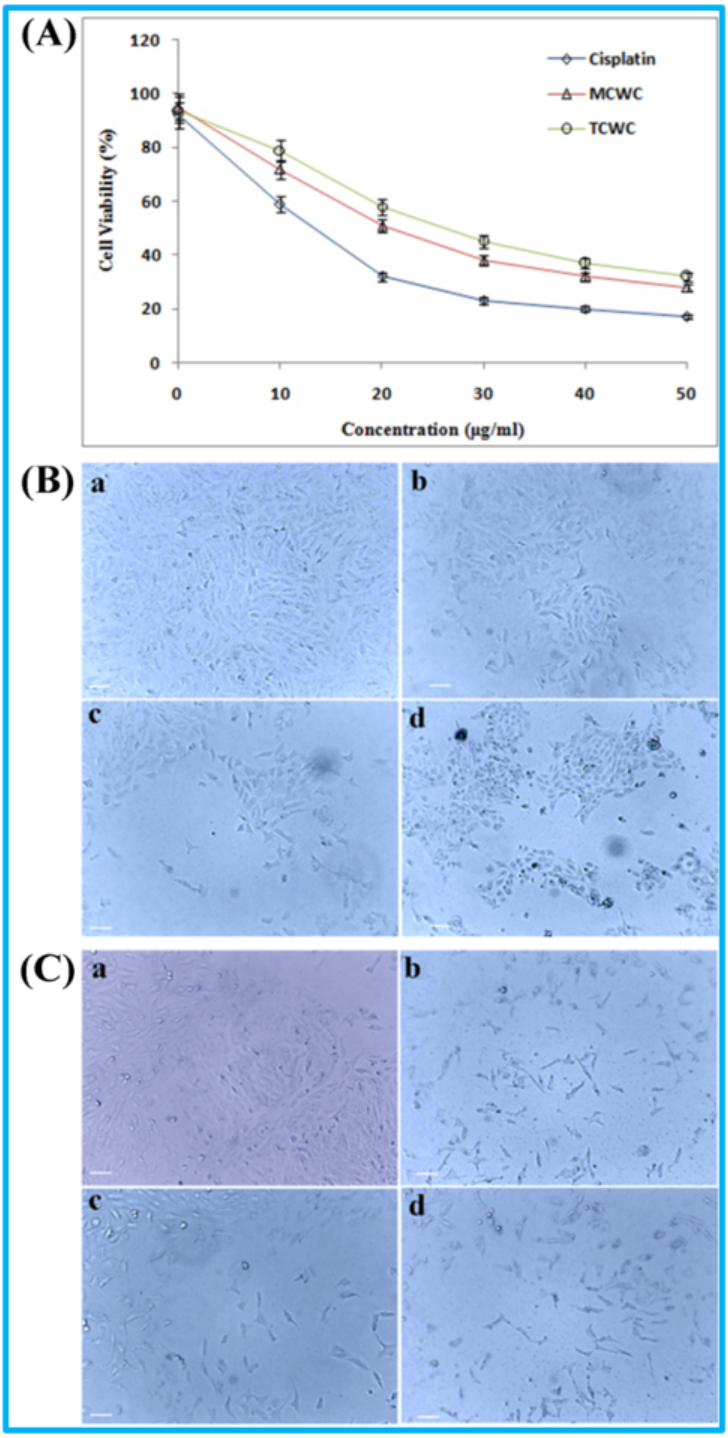

Figure 12

Figure 12

(A) Cytotoxicity in HeLa cells treated with TCW-Cu/Cu_2O-NS, MCW-Cu/Cu_2O-NS and standard drug Cisplatin; (B) Phase contrast microscopic images of HeLa cells (a) control (untreated) (b) 10 µg /ml (c) 25 µg/ml (d) 50 µg/ml treated with TCW-Cu/Cu_2O-NS (C) Phase contrast microscopic images of HeLa cells (a) control (untreated) (b) 10 µg /ml (c) 25 µg/ml (d) 50 µg/ml treated with MCW-Cu/Cu_2O-NS.

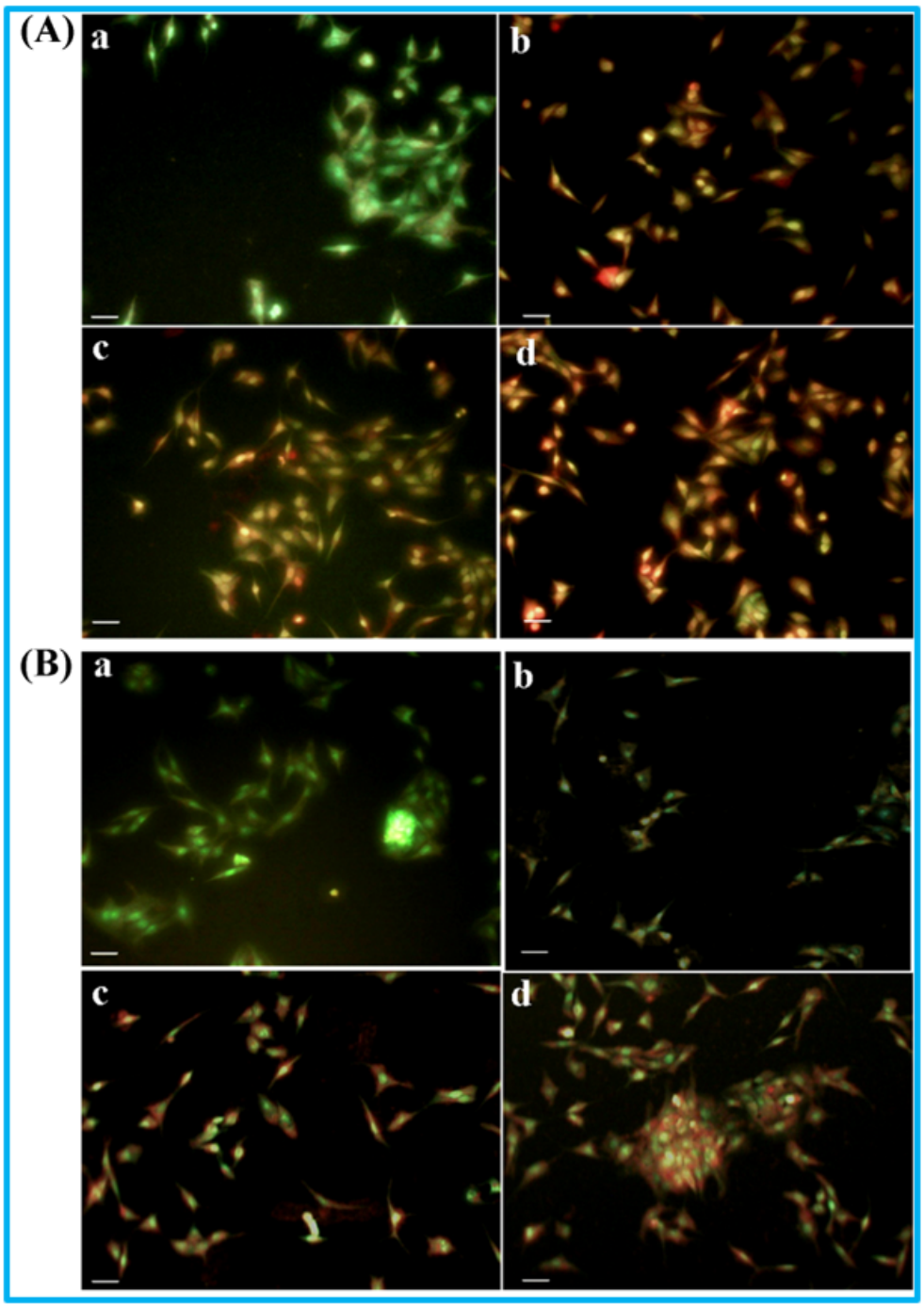

Figure 13

Figure 13

(B) Fluorescence microscopic images of A549 cells (AO/EB stained) (a) Control, (b) 10, (c) 25, (d) 50 µg/ml of MCW-Cu/Cu_2O-NS treated cells.

(A) Fluorescence microscopic images A549 cells (AO/EB stained) (a) Control, (b) 10, (c) 25, (d) 50 µg/ml of TCW-Cu/Cu_2O-NS treated cells.

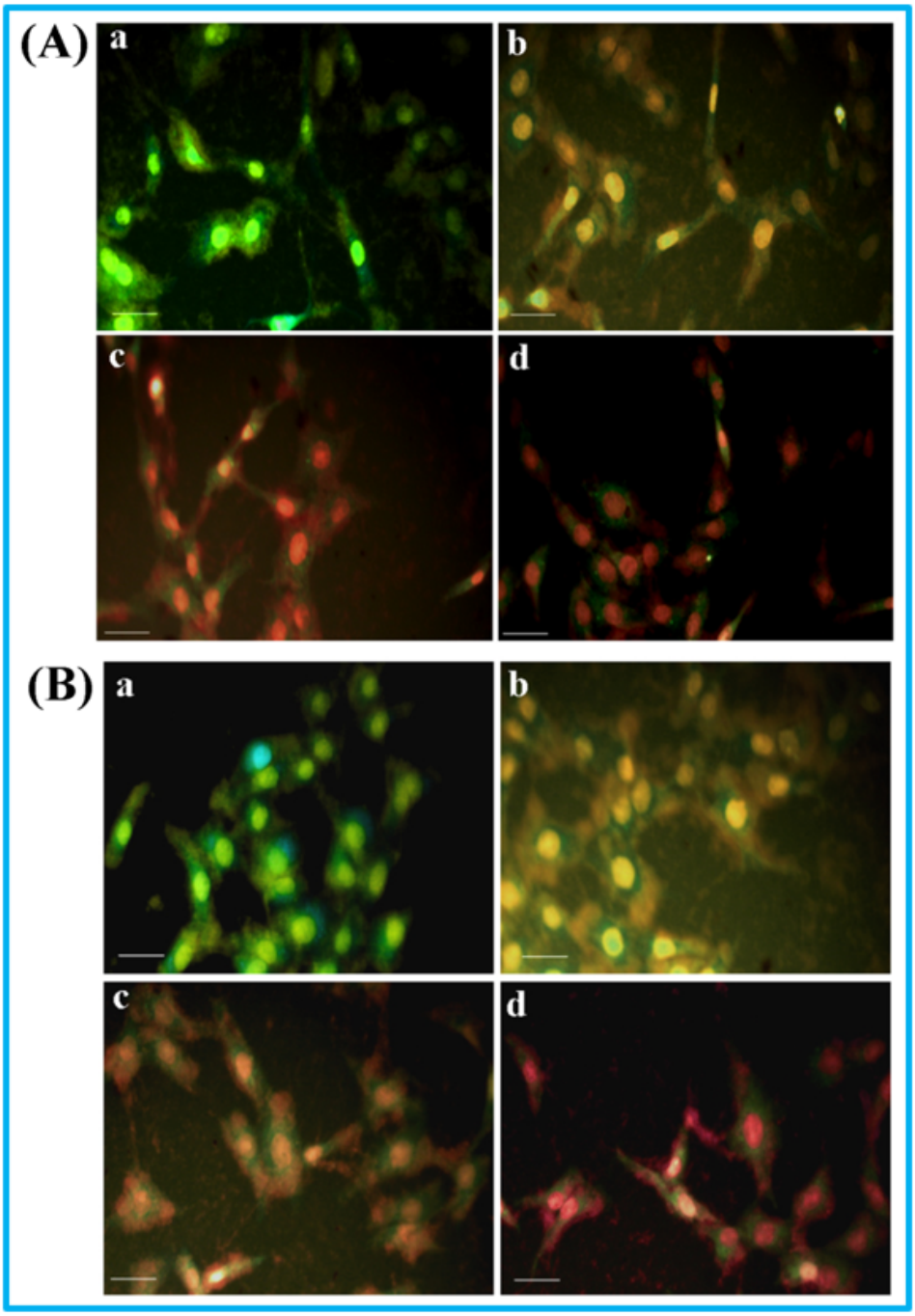

Figure 14

Figure 14

(A) Fluorescence microscopic images of HeLa cells (AO/EB stained) (a) Control, (b) 10, (c) 25, (d) 50 µg/ml of TCW-Cu/Cu_2O-NS treated cells.

(B) Fluorescence microscopic images of HeLa cells (AO/EB stained) (a) Control, (b) 10 (c) 25, (d) 50 µg/ml of MCW-Cu/Cu_2O-NS treated cells.

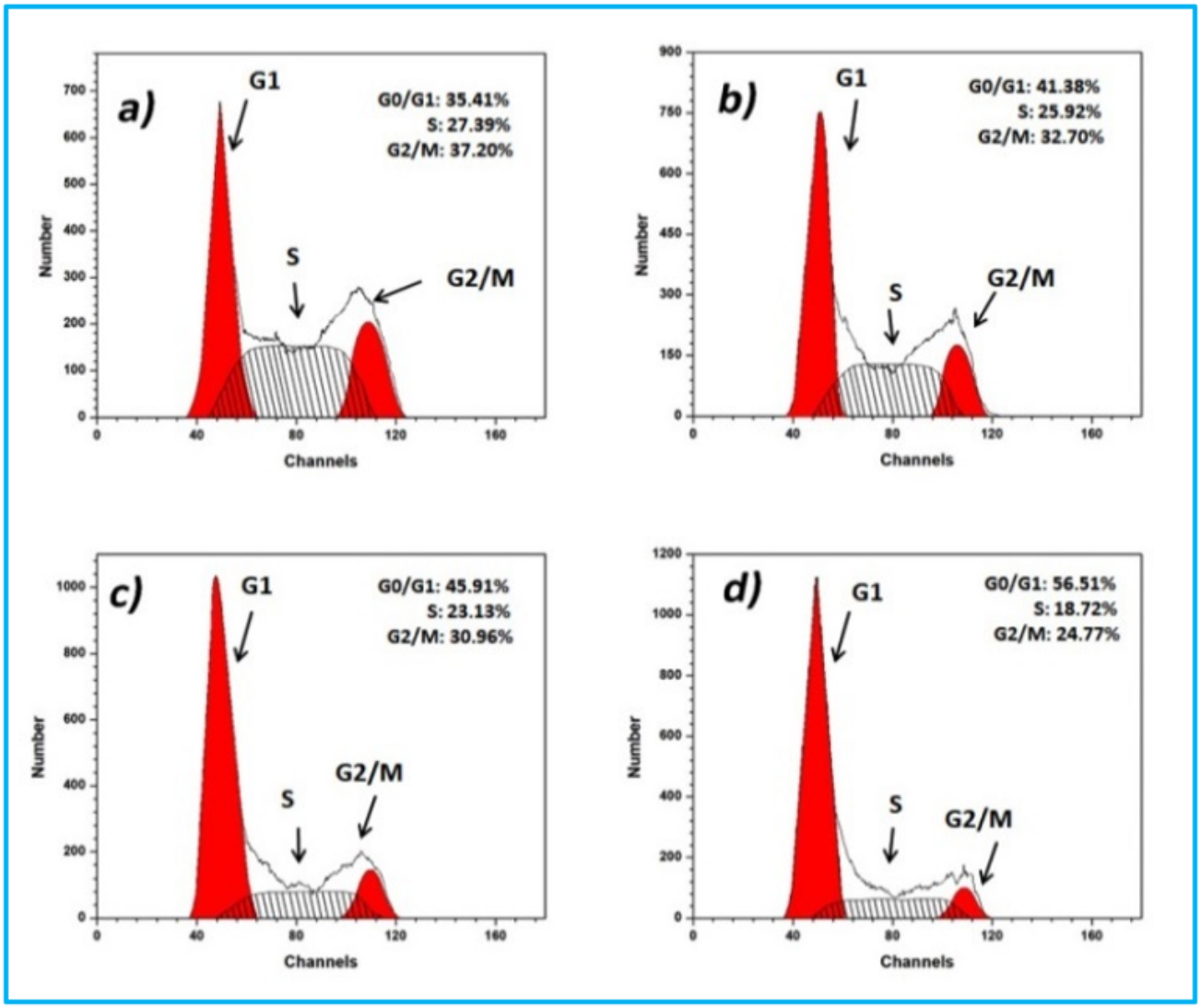

Figure 15

Figure 15

Apoptotic cell deaths in A549 cells analyzed by flow cytometry using Annexin–FITC/PI staining (a) control (untreated) and MCW-Cu/Cu_2O-NS (b) 10, (c) 25, and (d) 50 µg/mL.

Supplementary Files

This is a list of supplementary files associated with this preprint. Click to download.

- GA.png
- Scheme1.png

- SriniTCWMCWCuCu2ONSSupplementarydataJCS4.docx